具非等向性結構之鈀奈米晶體作為甲酸氧化之電化學觸媒研究

學生： 方郁歆　　指導教授：徐雍鎣 博士

國立交通大學

材料科學與工程學系

中文摘要

在此論文，我們成功利用一存在 PVP 水溶液的系統，以化學還原法合成出不同形狀的鈀奈米晶體，包括奈米板狀，八面體，孔狀和中空狀。我們使用 $PdCl_2$ 當前驅物而 PVP 扮演還原劑和穩定劑，另外我們加入一些特定的鹽類如 NaCl 和 NH_4OH。在此合成系統中，鈀奈米晶體之形貌與尺寸可藉由相關反應條件之操控來調整，例如 $PdCl_2$ 和鹽類的莫耳數和反應溫度。我們將四種不同鈀奈米型狀應用電化學活性中的甲酸氧化和氫氣的吸脫附，我們可以發現不同的形狀在甲酸氧化有不同的現象。非等向結性構的鈀奈米晶體亦應用在表面增強拉曼，由於鈀奈米形狀不同影響有機分子在拉曼的靈敏度，

Anisotropic Palladium Nanocrystals as Electrocatalyst for Formic Acid Oxidation

Student： Yu-Sin Fan Advisor：Dr. Yung-Jung Hsu

National Chiao Tung University

Department of Materials Science and Engineering

Abstract

In this thesis, we successfully synthesized various palladium (Pd) nanocrystals including nanoplates, octahedrons, porous nanocrystals, and hollow nanocrystals in the PVP-assisted chemical reduction process. The synthesis involved only the use of $PdCl_2$ as the precursor, PVP as the reducing and stabilizing agents, and a specific salt like NaCl or NH_4OH as the additive. By modulating the relevant reaction conditions such as the amount of $PdCl_2$, the amount of additive, and the reaction temperature, we were able to obtain Pd nanocrystals with controllable morphologies. The four types of Pd nanocrystals exhibited notable electrocatalytic activities toward formic acid oxidation and hydrogen adsorption/desorption. Surface-enhanced Raman spectroscopy for the

anisotropically-shaped Pd of nanoplates and octahedrons was also investigated to demonstrate their potential as an active substrate for Raman-sensitive analyte molecules.

致謝

很高興能在這七百多個日子後的今天寫這篇致謝，首先感謝我的指導教授徐雍鎣博士，感謝老師不厭其煩的指導與討論，在老師的引導下才能順利的寫出論文。另外也感謝，李建良教授和羅介聰教授對我論文的指導，使得論文更加正確與完整。

謝謝實驗室的大家一起陪我渡過，當實驗上遇到瓶頸感到沮喪時，大家的笑聲是趕走討厭的煩躁感最好的方法。感謝各位學長的幫忙，無論在儀器的操作上或是實驗上的討論，謝謝你們的鼎力相助讓我克服重重的困難。還有感謝我的同學陳宇志和 Ann，感謝你們一路陪伴和幫忙。還有謝謝學弟妹們的幫忙，有你們實驗室總是充滿的歡樂。

最後謝謝一路支持我的家人，此論文獻給我最愛的家人。

Table of Content

Figure Captions

Table Captions

Chapter 1. Introduction

1.1 Palladium Nanocrystals

Metal nanoparticles continue to attract immense attention because of their unusual optical sensing, biosensing,[1] catalysis,[2] magnetic, electrical properties[3] and also surface-enhanced Raman scattering (SERS)[4]. Morphology-controlled synthesis of nanocrystals has attracted much attention because the size and morphology of most nanocrystals have a great effect on their chemical and physical properties. In the past decade, significant progress has been made in the development of new synthetic methods for metal nanocrystals, and various morphologies have been fabricated. Among these nanostructures, single-crystalline nanocrystals have received much attention.

Compared to the more extensively studied metal materials such as Ag and Au, many properties of Pd still have not been widely examined. Pd, which is a face-centered cubic noble metal, is often used as primary catalysts for the low temperature reduction of automobile pollutants and organic reactions such as Suzuki, heck coupling, and it has prominent performance in hydrogen adsorption and sensing. Significantly, Pd

nanostructures, which have larger surface area-to-volume ratio and more active centers, have been used in various electrochemical reactions.[5] Recent, Pd-based catalysts boosts the performance of direct formic acid fuel cells to better levels than that observed with Pt based catalysts. It is believed that the lack of CO poisoning on Pd catalysts leads to higher activity than Pt-based catalysts.[6]

1.2 Studies about Pd Nanorods

Most of shape-controlled syntheses for nanocrystals involve the reduction of salt precursors or thermal decomposition of organometallic compounds in the presence of organic surfactants, polymers, coordinating ligands, adding foreign ionic species, and mediation of seed. In recent years, Xiong et al reported 1-D Pd nanorod in aqueous solution phase.[7] The single-crystals Pd nanorods were synthesized by dissolving Na_2PdCl_4, PVP and KBr in ethylene glycol and then heating the reaction mixture. The Pd precursor was reduced by ethylene glycol and PVP. Here PVP serves as a mild reducing agent for the generation of metal nanoparticles. In contrast to the weak reducing strength of PVP, EG was a more powerful reducing agent for the reduction of a metal salt. When increased the EG

concentration, reaction rate was enhanced. Through this kinetic control, the reaction can generate nanobars and nanorods with different aspect ratios (see Figure 1.1). More faster reduction rate induces anisotropic growth for the nanocrystals. In this synthesis, addition of bromide at a sufficiently high concentration could cover the surface of a Pd nanocrystal with bromide due to its strong chemisorbing to the Pd surface. Bromide layer prevents Pd atoms in solution from getting to the nanocrystal surface, so one has to activate the surface of this nanocrystal to continue the growth. Figure 1.2 show the products obtained by using different KBr concentrations.

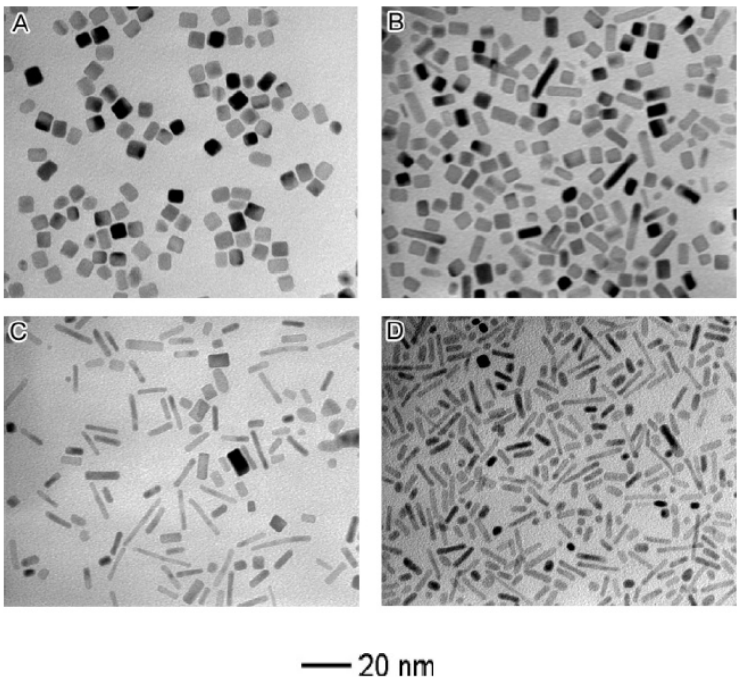

Figure 1.1 TEM images of Pd nanocrystals obtained by adjusting the volume percent of ethylene glycol in the solvent mixture: (A) 0%, (B) 9.1%, (C) 45.5%, and (D) 72.7%. The reaction temperature was 100 °C.[7]

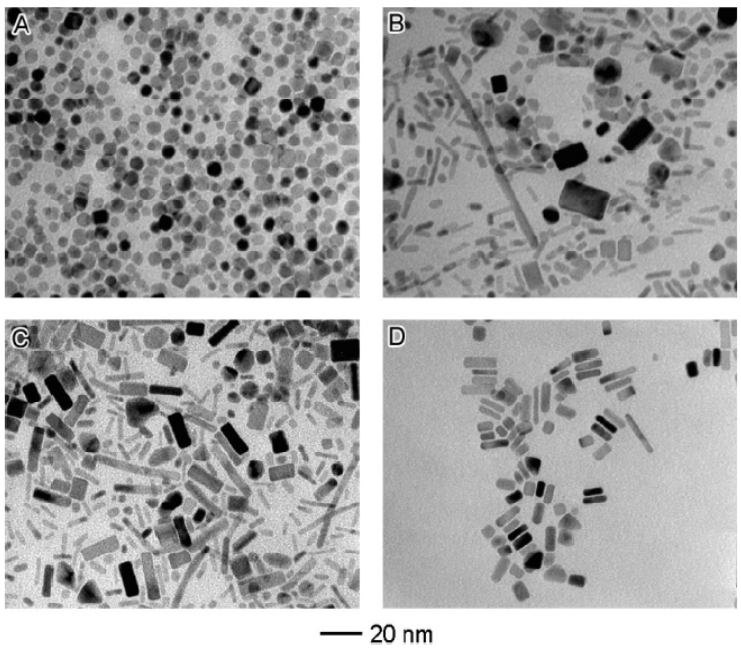

Figure 1.2 TEM images of Pd nanocrystals synthesized in the presence of KBr at different concentrations, demonstrating the role of bromide in promoting {100} and {110} surfaces. The molar ratio of KBr to Na_2PdCl_4 was: (A) 0, (B) 8, (C) 15, and (D) 50.[7]

1.3 Studies about Pd Nanocubes and Twin Particles

The hydrothermal method is another way to synthesize Pd nanocrystals. Zheng and coworker discussed the halide effect in the formation of metal nanoparticles.[8] Nanocubes and twin particles of Pd can be relatively obtained in the presence and absence of I^- ions. Figure 1.3 shows the corresponding TEM images of the products. The dimensions of the twinned particles prepared using other halides (F^-, Cl^-, or Br^-) are in the order of $F^- > Cl^- > Br^-$; however, they are all smaller in size than those synthesized without halide (see Figure 1.4).

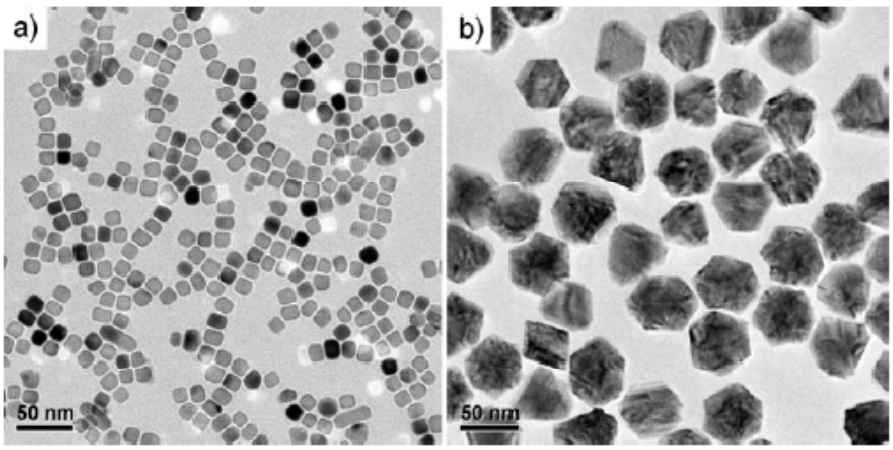

Figure 1.3 TEM images of Pd nanocrystals: (a) nanocubes prepared with the use of I^- ions; (b) twinned particles prepared without the use of any halide.[8]

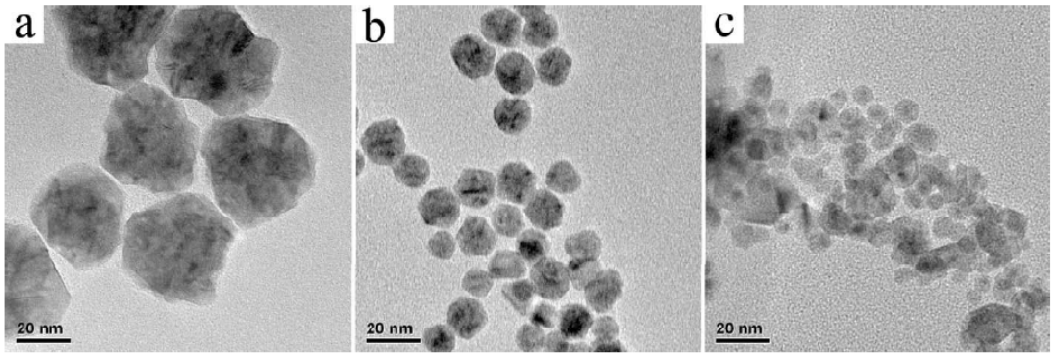

Figure 1.4 TEM images of Pd nanocrystals by using the same conditions for the synthesis of Pd nanocubes but with I^- replaced by (a) F^-, (b) Cl^-, and (c) Br^-.[8]

1.4 Studies about Pd Nanoplates and Polyhedrons

Xiong et al demonstrated that oxidative etching by Fe(III) species and the $Cl^-/O_2$with polyol reduction induce the formation the triangular and hexagonal nanoplates of Pd.[9] they found that the percentage of Pd triangular nanoplates in the final product was strongly depend on the molar ratio between PVP and Pd precursor. As shown in Figure 1.5, when this ratio was around 5, the content of Pd triangular nanoplates could approach 70%. However, if the ratio was decreased or increased to other values, the yield of Pd nanoplates in the final product would drop. They concluded that the surface of nanocrystals with less PVP was easily etched so that their morphology was affected. A large amount of PVP would probably passivate the {100} side faces of nanoplates and the twinned particles could be grown through etching by the Cl^-/O^2 pair, resulting in small lateral dimensions. Etching of O_2/Cl^- pair could not sufficiently slow the reduction to achieve anisotropic growth and form thin nanoplates. They solve this problem by adding ferric species to the reaction solution. In this system, Fe(III) could oxidize Pd^0 back to Pd^{2+}, competing with the formation of Pd^0, and thus reducing the overall

formation rate of Pd^0. Figure 1.6 shows that the morphology of final product were strongly dependent on the concentration of $FeCl_3$

Figure 1.5 TEM images of Pd nanocrystals obtained by using different molar ratios of PVP to Pd precursor: (A) 1, (B) 5, (C)25.[9]

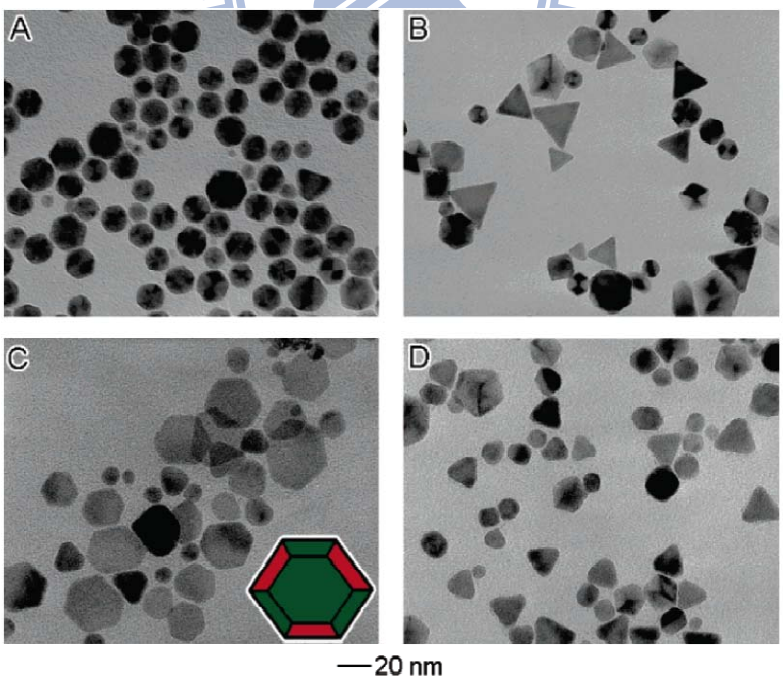

Figure 1.6 TEM images of Pd nanocrystals obtained by adding $FeCl_3$ of different concenrations (molar ratio of PVP to Pd precursor is 5): (A) no $FeCl_3$, (B) 0.18 mM, (C) 0.72 mM, (D) 0.36 mM $FeCl_3$ in Ar.[9]

Xu et al synthesized single-crystalline Pd nanocrystals with varying shapes by using the seed-mediated strategy.[10] Through manipulation of the concentration of KI and the reaction temperature, several types of Pd nanocrystals were synthesized. Figure 1.7 shows the Pd nanocrystals obtained with varying KI concentrations and reaction temperatures. At either very low or relatively high KI concentration, the {100} Pd facets are favored. In the medium KI concentration, the {110} Pd facets are favored at relatively high temperatures. The {111} Pd facets are favored at relatively low temperatures and medium KI concentrations.

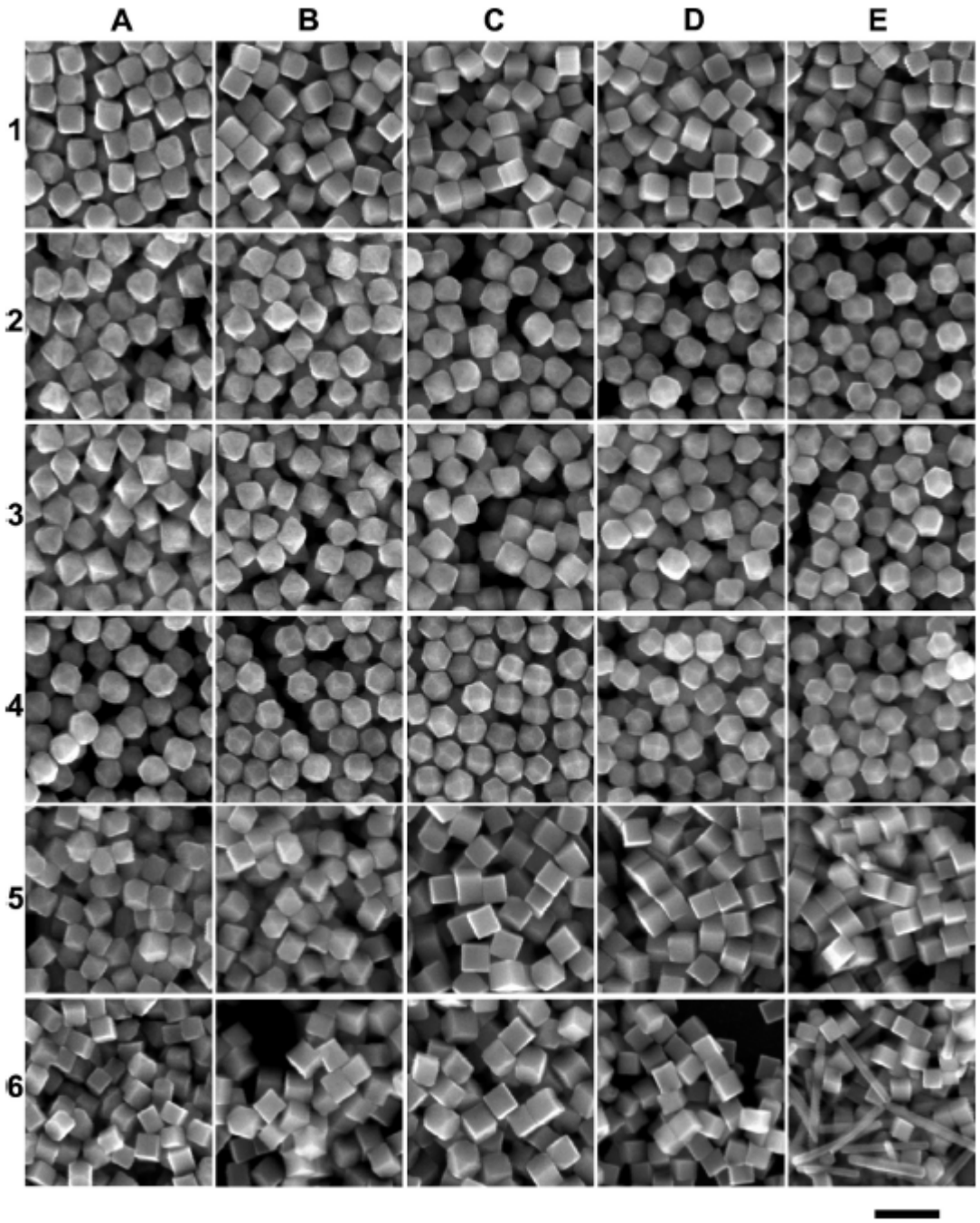

Figure1.7 SEM images of polyhedral Pd nanocrystals synthesized under different conditions (scale bar is 200 nm). In columns A-E, the reaction temperatures are 30, 40, 50, 60, and 80 °C, respectively. In rows 1-5, 5μL of 100 mM, 5μL of 10 mM, 25μL of 1 mM, 5 μL of 1 mM, and 5μL of 0.1 mM KI solutions were added to the growth solutions, respectively. In row 6, no KI was added.[10]

1.5 Studies about Branched Pd Nanocrystals

Three-dimensional branched nanocrystals are promising candidates as they possess a large surface area available for reaction. Using Pd precursor with a mixture of oleylamine and oleic acid (1:1 in molar ratio), the synthesis of Pd can be performed at room temperature under 3 bar hydrogen for 160min of reaction.[11] Figure 1.8 shows the morphological evolution of branched Pd nanocrystals with different reaction times. If only oleyamin was used, only polyhedral particles were formed. While oleic acid with the weaker binding function groups could reduce the overall degree of surface stabilization of the growing particles, the addition of oleic acid in reaction favored the formation of highly branched structures of Pd (see figure 1.9).

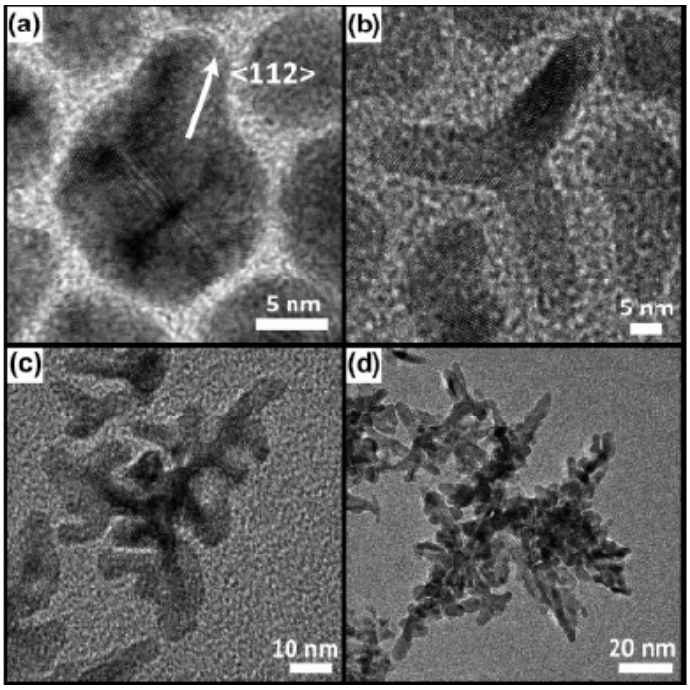

Figure1.8 TEM images showing the evolution of branched Pd nanocrystals: (a) icosahedra with small leg beginning to grow in the [112] direction; (b) tripod-shaped nanocrystal formed after 30 min; (c) intermediate morphology after 80 min; and (d) fully developed nanostructure after 120 min.[11]

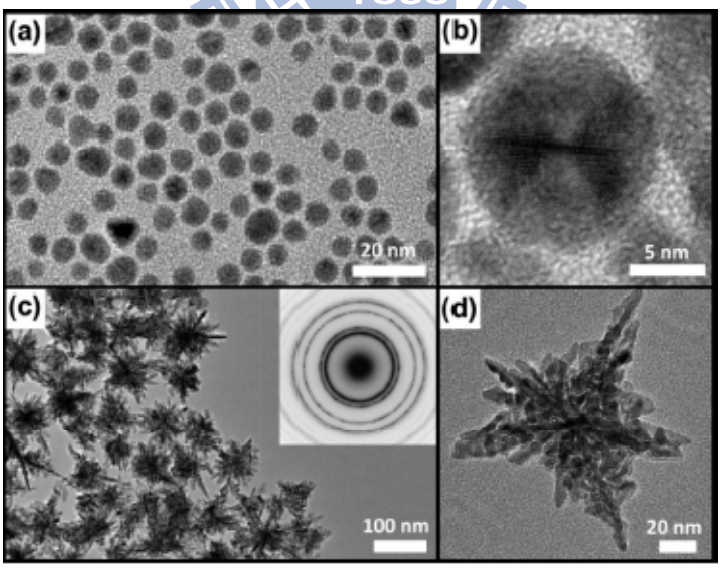

Figure1.9 TEM images of (a) (b) polyhedral Pd nanocrystals formed using pure oleylamine, and (c) (d) highly branched Pd nanocrystals formed using a 1:1 mixture of oleylamine and oleic acid.[11]

1.6 Applications of Pd Nanocrystals

Pd plays a key role in technologies for hydrogen storage[12], organic reaction[13] such as Suzuki and Heck and hydrogenation.[14] Because of a large surface-to-volume ratio of nanocrystals, Pd nanocrystals provide higher catalytic efficiency per gram than their bulk crystals. The other applications that have been extensively studied for Pd nanocrystals were fuel cell and their surface-enhanced Raman scattering (SERS) properties.

1.6.1 Pd-based Electrocatalysts for Oxidation of Formic Acid

In the past several decades, many model catalysts, such as single crystal Pt,[15] Pt-based metal alloy[16] and Pt modified with other metal/non-metal have been investigated. Recently, it was found that Pd catalysts produced unusually high performance in active direct formic acid fuel cells.[17,18] Pd not only exhibits high catalytic activity for formic acid oxidation, but also overcomes the CO poisoning effect. Elucidation of surface structures enhancing the activity for electrochemical reactions will contribute to the development of new electrocatalysts with high efficiency and low energy consumption. Since the electrocatalytic activity strongly depends on the shape of metal nanocrystals,[19]

morphology-controlled synthesis of Pd with tailored shape and size is highly desirable. Besides, surface structure of Pd affects the catalytic activity and the selectivity of electrochemical reactions remarkably.

The research on the electrocatalysts for formic acid oxidation is crucial for the development of direct formic acid fuel cells.[20] A simple and environmental friendly method has been proposed to obtain Pd nanowire networks that exhibit a high electrochemical activity toward formic acid oxidation (see Figure 1.10). In this paper, the electrocatalytic activity of Pd nanowires for formic acid oxidation was compared with that of Pd nanoparticles. The result was shown in Figure 1.11. The forward peak current for formic acid oxidation on Pd nanowires was 2.86 mA cm^{-2}, which was significantly higher than 0.97 mA cm^{-2} of that on Pd nanoparticles. The electrochemical active surface areas were determined from CO stripping voltammetry in 0.5 mol/L H_2SO_4. The electrochemical specific surface areas of the Pd nanoparticles and nanowires were estimated to be 615.2 and 585.4 cm^2 mg^{-1}, respectively, from the integration of the stripping charge. The final products of Pd nanowires exhibited a superior catalytic activity for formic acid oxidation. The template free and environmentally friendly method was a very attractive

way to produce Pd nanowires for use in formic acid fuel cells.

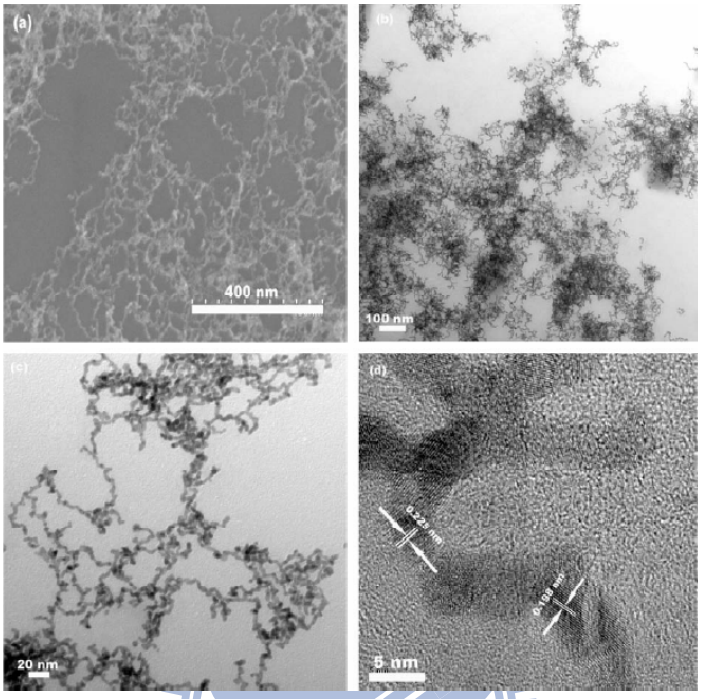

Figure1.10 (a) SEM image, (b)-(d) TEM images of Pd nanowire network.[20]

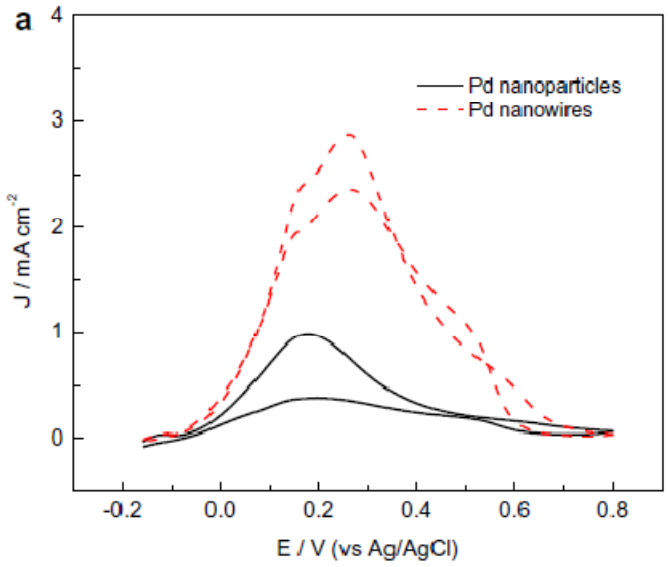

Figure 1.11 CV plots with a scan rate of 20 mV/s for Pd nanoparticles and Pd nanowire network recorded in 0.5 M HCOOH + 0.5 M H_2SO_4 solution.[20]

Hoshi et al elucidated surface structures enhancing the activity toward electrochemical reactions would contribute to the development of Pd electrocatalysts with high efficiency and low energy consumption.[21] Figure 1.12 shows the voltammograms of formic acid oxidation in 0.1M $HClO_4$ containing 0.1M formic acid. The maximum oxidation rate depended on crystal plane of Pd remarkably: Pd(110) < Pd(111) <Pd(100). For Pd, its (100) plane had the highest oxidation rate of formic acid. Comparison of Figure 1.12a with Figure 1.12b shows that formic acid oxidation needs no oxygen donor on Pd electrodes. On Pd(100), PdOH(Pd_2O) is formed at 0.7 V, but the onset potential of formic acid oxidation is far more negative at 0.2V. The current of formic acid oxidation drop at 0.83V, and become to zero at 1.0V. From the result shown in Figure1.12b, they deduced that first layer of Pd(100) was fully covered with PdOH(Pd_2O) at 1.0V. These results indicated that oxygen donor on the surface inhibited the oxidation of formic acid on Pd(100). Low index planes of Pd may give sharp anodic peaks at the potentials where most of the oxide film is reduced in the negative scan. A previous study reported that the reduction of the oxide film of Pd activated the oxidation of formic acid on Pd polycrystalline electrodes.[22]

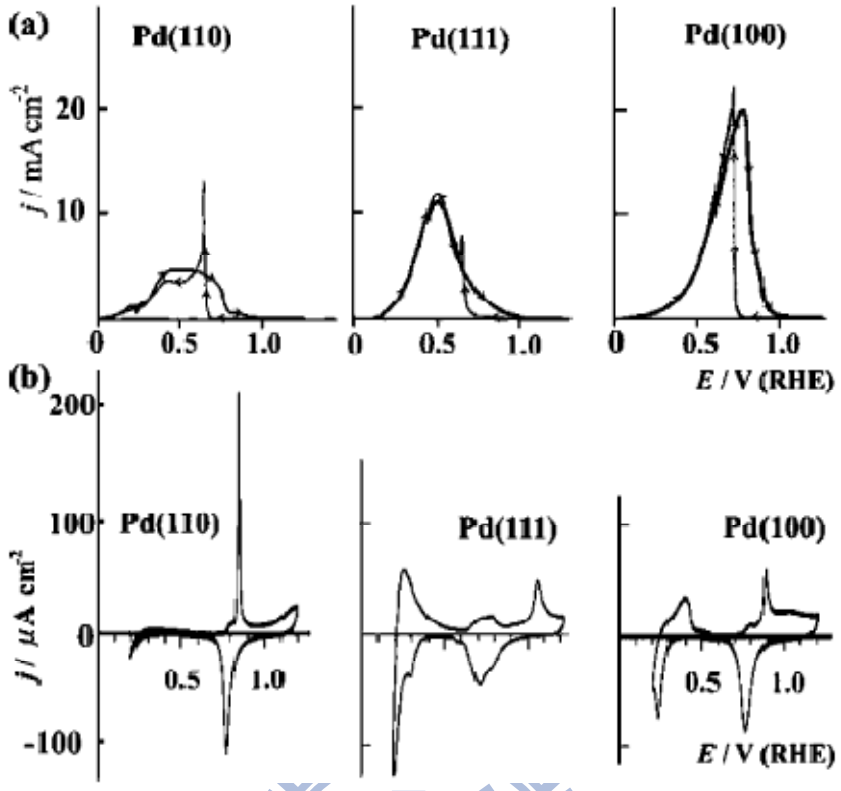

Figure1.12 CV plots for Pd with different planes recorded (a) in 0.1 M $HClO_4$containing 0.1 M formic acid, and (b) in 0.1 M $HClO_4$ without formic acid.[21]

1.6.2 SERS Properties

Different shapes of Pd nanocrystals would show different degree of enhancement in SERS signal.[23] It has been widely accepted that there are two primary mechanisms in SERS enhancement: one being electromagnetic enhancement that arises from the extremely high local fields due to surface plasmon resonance (SPR), and the other being chemical enhancement due to resonance Raman-like interaction between the substrate and the adsorbate. As shown in Figure 1.13, the intensity of

SERS of 4-mercaptopyridine signals from Pd nanocubes of 50 nm in edge length was stronger than those of 8 and 25 nm. In addition, the SERS intensity was greatly enhanced as the SPR band of these particles was red-shifted. They also investigated the efficiency of Pd hollow nanoparticles in SERS such as hollow boxes and cages with edge lengths of ~50 nm that have even more red-shifted SPR bands. They found that the nanoboxes gave the strongest enhancement among all the samples (Figure 1.14).

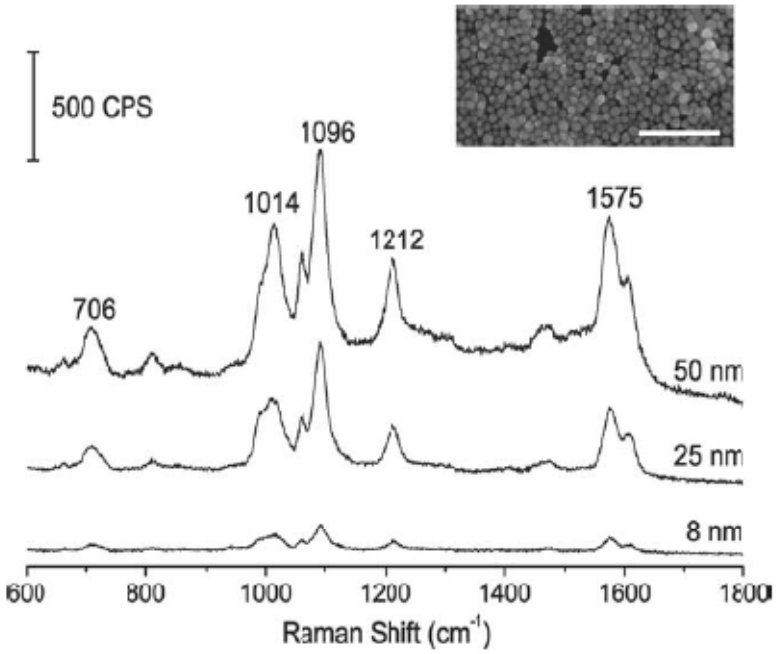

Figure 1.13. SERS spectra of 4-mercaptopyridine adsorbed on films of Pd nanocubes with 50, 25, and 8 nm of edge lengths. The inset shows a typical SEM image of the thin film containing 50 nm Pd nanocubes. The scale bar is 500 nm.[23]

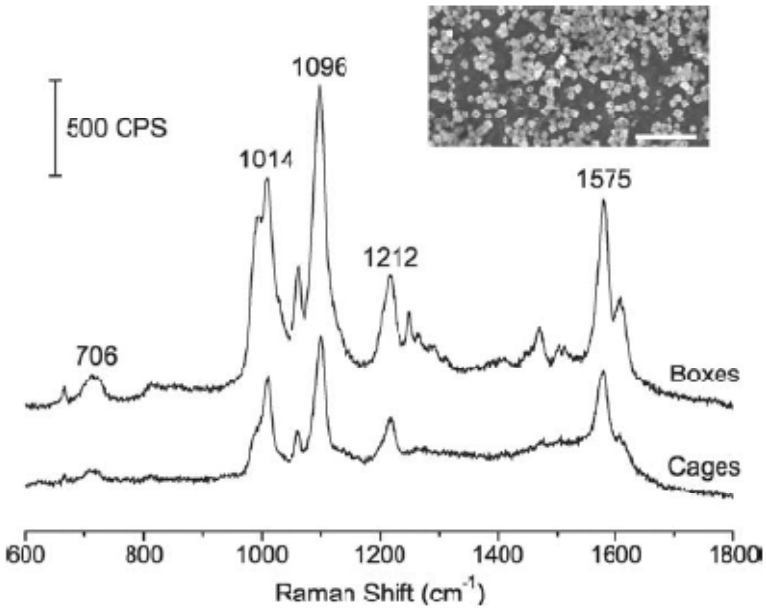

Figure 1.14. SERS spectra of 4-mercaptopyridine adsorbed on thin films of Pd nanoboxes and nanocages. The inset shows a typical SEM image of the film containing 50 nm nanoboxes. The scale bar is 500 nm.[23]

Chapter 2. Experimental Section

2.1 Chemicals

All chemicals were analytic grade reagents and used without further purification.

1. Palladium(II) Chloride($PdCl_2$), 99%, UR-IPAL001
2. Polyvinpyrrolidone (PVP), MW=29,000, Aldrich
3. Sodium Chloride (NaCl), Crystal, J.T.Baker
4. Ammoniumhydroxide (NH_4OH), 30-33%, Sigma-Alorich
5. Sulfuric Acid (H_2SO_4), 96%, Osaka
6. Perchloric Acid ($HClO_4$),70%-72%, Guaranteed
7. Formic Acid (HCOOH), 98%, Riedel-deHaen
8. Commercial Pd, Pd on carbon, 10 wt.%, Aldrich
9. Methylene Blue ($C_{16}H_{18}N_3SCl \cdot 3H_2O$), Aldrich

2.2 Instruments and Principles

1. Scanning Electron Microscope (SEM): The kinetic energy of accelerated electrons in SEM is dissipated as many different signals when hitting the sample surfaces. These signals mainly include

secondary and backscattered electrons. Secondary and backscattered electrons are then collected and used for imaging the morphology and compositional contrast of samples, respectively.

2. Transmission Electron Microscope (TEM): In TEM, the electrons are focused with electromagnetic lenses and transmitted through the sample to image and analyze the microstructure. The electron beams are basically accelerated at several hundred kV, producing wavelength much smaller than that of light. For example, 200 kV of acceleration voltage produces electron beam with a wavelength of 0.025Å. The resolution of TEM is however limited by aberrations inherent in electromagnetic lenses, which is about 1-2 Å.
3. Cyclic Voltammetry (CV): CV is generally used to study the electrochemical properties of the analyte in solution. It is composed of the reference electrode, the working electrode, and the counter electrode and is usually referred to as a three-electrode setup. The current at the working electrode is recorded with the applied voltage to give the CV trace. The range of the potential depends on the types of solvent, electrolyte and specific working electrode materials used.
4. Raman Spectroscopy: Raman spectroscopy is a technique used to

study the vibrational, rotational, and other low-frequency bonding modes in materials. It involves the inelastic scattering or Raman scattering of monochrfomatic light that comes from a laser in the visible, near infrared, or near ultraviolet range. The laser light interacts with phonons and excitations in the sample, which leads to the up- or down-shifting in the energy of the laser photons. This shift gives information about the phonon modes in the system. The frequency of light scattered from a molecule is related to the structural characteristics of the molecular bonds.

5. X-Ray Diffraction (XRD): In XRD, a constructive interference is produced through the interaction of the incident X-ray with the sample under the regime of Bragg's Law ($n\lambda = 2d \sin\theta$). This law correlates the wavelength of X-ray (λ) with the diffraction angle (2θ) and the lattice spacing of crystal (d) of the sample. By scanning the sample through a wide 2θ range to collect primary diffraction peaks, one may identify the crystal structure of sample by referring to the standard reference patterns.

2.3 Synthesis with Various Amounts of $PdCl_2$

In a typical synthesis, a 0.01M PVP (MW: 29000) solution was first prepared and stored at room temperature. $PdCl_2$ powder of various amounts (0.1, 0.3, 0.5, and 1.0 mmol) was evenly dispersed in 20ml deionized water. The solution was then added into 0.3 mL of PVP solution. After standing at 100℃ for 15 h, the solution turned dark brown in color. The products were collected by centrifugation at 15000 rpm for 5 min and washed with distilled water and ethanol to remove remaining ions and surfactants. The washed product was stored in ethanol for later characterization and use.

2.4 Synthesis with Addition of NaCl or NH_4OH

To increase the solubility of $PdCl_2$ in water, NaCl (1.0 M) or NH_4OH (1.0 M) was added along with $PdCl_2$ in water when preparing the solution containing Pd^{2+} ions. In a typical synthesis, $PdCl_2$ of 0.3 mmol along with NaCl of various amounts (0.1, 0.5, 1.0 mL) were dispersed in deionized water with a total volume of 20 mL. After standing at 75℃ (or 100℃) in water bath for 15 h, the solution turned brick red. The products were collected by centrifugation at 15000 rpm for 5 min and washed with

distilled water and ethanol to remove remaining ions and surfactants. For the addition of NH_4OH, various amount of NH_4OH (0.1, 0.3, 1.0 mL) were employed, followed by the same procedure used in NaCl case except for the reaction temperature set at 85℃ (or 100℃). The solution color turned light yellow after the reaction was completed.

2.5 Preparation of Pd Electrode

To prepare electrode for CV measurement, a drop of solution containing Pd nanocrystals of 0.05 mg was dried on the FTO substrate (10 mm×10 mm) and used as the working electrode. The amount of Pd in solution was determined from ICP-MS analysis. Before the CV measurement, the working electrode was heated at 300℃ in N_2 atmosphere for 2 h to remove the excess PVP that covered at the surfaces of nanocrystals.

2.6 Preparation of Raman-active Substrate

SERS substrate was prepared by dripping nanocrystal solutions with a fixed amount on Si wafer. After completely dried, the substrate was

immersed in a methylene blue solution (MB, 0.5 mM) for 10min. The sample was then taken out, rinsed with deionized water to remove any unadsorbed MB molecules, and dried in 60℃ for later use.

2.7 Characterizations

The morphology of the products was examined with a field-emission SEM (FESEM, Jeol, JSM-6500F) and a high-resolution TEM (HRTEM, Jeol, JEM-2010) operated at 200 kV. The crystallographic structure of the samples was investigated with XRD (Burker, D2 phaser). CVs were recorded using Jiehan 5600 potentialstat at room temperature in 0.5M sulfuric acid solution and in 0.5M perchloric acid + 2.0M formic acid solution. These solutions were degassed with N_2 prior to the measurement. Pt and Ag/AgCl in saturated KCl were served as the counter and reference electrodes, respectively. Inductively Coupled Plasma-Mass Spectrometer (ICP-MS, Perkin Elmer, Sciex Elan 5000) was employed to determined the amount of Pd in nanocrystal solutions. Raman spectra were obtained using a LABRAM HR 800 spectroscope equipped with He/Ne laser (632.8nm).

Chapter 3. Results and Discussion

3.1 Effect of $PdCl_2$ Amount

In the current synthetic approach, PVP could reduce Pd^{2+} to form Pd^0 with its hydroxyl groups. More importantly, the oxygen and nitrogen atoms of the pyrrolidone unit could facilitate the adsorption of PVP onto Pd{111}, making PVP a good stabilizer to protect nanocrystals from agglomeration. Figure 3.1.1 shows the morphologies of Pd nanocrystals obtained with different amounts of $PdCl_2$. Plate-like structures with tiny size (50~100 nm in edge length) were first observed in the product when $PdCl_2$ of 0.1 mmol was used. This plate-like structure resulted from the capping effect of PVP during the crystal growth of Pd. It should be noted that nanoplates are intrinsically unstable in crystal growth since they are not thermodynamically favored shapes. It has been pointed out that the formation of metal nanoplates would become favorable once the reduction of metal ions took place in a relatively slow rate.[24] PVP was a weak reducing agent as compared to ascorbic acid and ethlylene glycol, which is an important factor in kinetically promoting the formation of nanoplates here. The yield of nanoplates can be significant enhanced as

increasing the amount of $PdCl_2$ to 0.3 and 0.5 mmol. This is due to the decreasing ratio of PVP to $PdCl_2$ which may prevent the over-coverage of PVP on each Pd nanocrystal to improve the steadiness of the crystal growth. Besides, these nanoplates were larger in size (100~150 nm) than those obtained using 0.1 mmol of $PdCl_2$. This outcome originated from the lower ratio of PVP to $PdCl_2$ that caused less pronounced steric hindrance to facilitate the growth of Pd. When the amount of $PdCl_2$ was further increased to 1.0 mmol, Pd nanocrystals with irregular shapes were obtained. The insufficient PVP molecules which were not able to fully passivate the {111} plates of Pd may account for such irregular morphology observed.

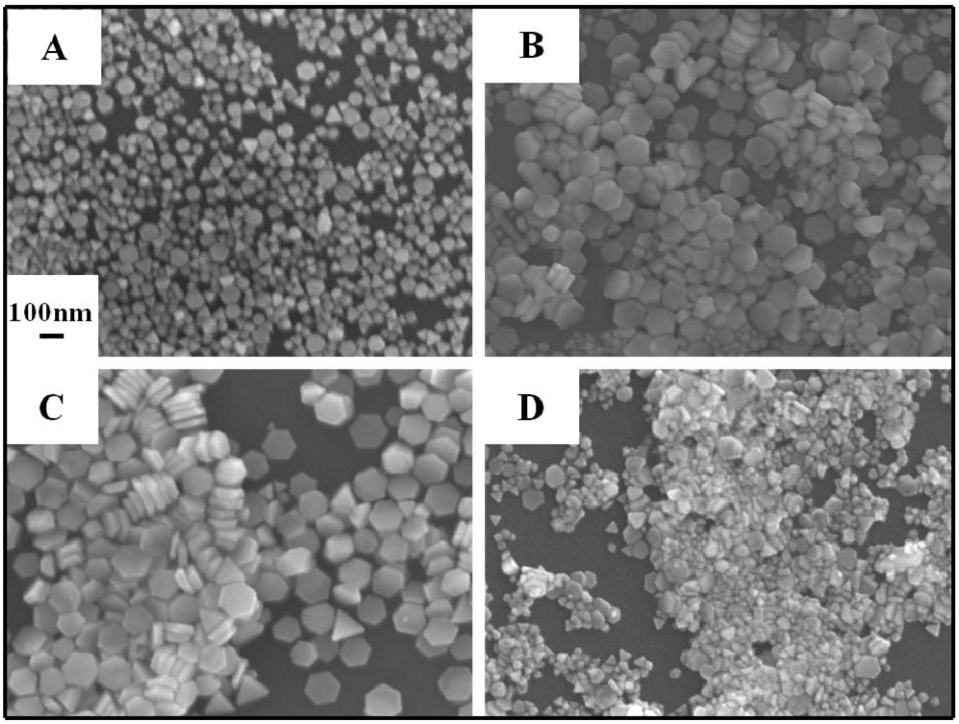

Figure 3.1.1. SEM images of Pd nanocrystals obtained by using $PdCl_2$ of (A) 0.1, (B) 0.3, (C) 0.5, and (D) 1.0 mmol.

XRD and TEM measurements were then performed to study the crystallographic structure of these Pd nanocrystals. The result of XRD analysis shows that the as-synthesized Pd nanocrystals were face-centered cubic (FCC) structure with the (111) peak showing much stronger intensity than the others. This phenomenon indicates that the present nanoplates of Pd were composed of {111} planes at their top surfaces and {110} at their lateral facets. This proposition can be confirmed by the corresponding HRTEM and SAED analyses shown in Figure 3.1.2. The HRTEM image of Figure 3.1.2(B) clearly reveals three identical {-220}

planes with the interlayer spacing of 0.14 nm. The inset SAED pattern can be indexed as the fcc Pd crystal projected along the [111] zone axis. This result, together with those of SEM and XRD analyses, confirms our proposition that Pd nanoplates were composed of {111} and {110} at the top and lateral surfaces, respectively. The intensity ratios of (111) to (200) peaks for the four samples collected here were summarized in Table 1.

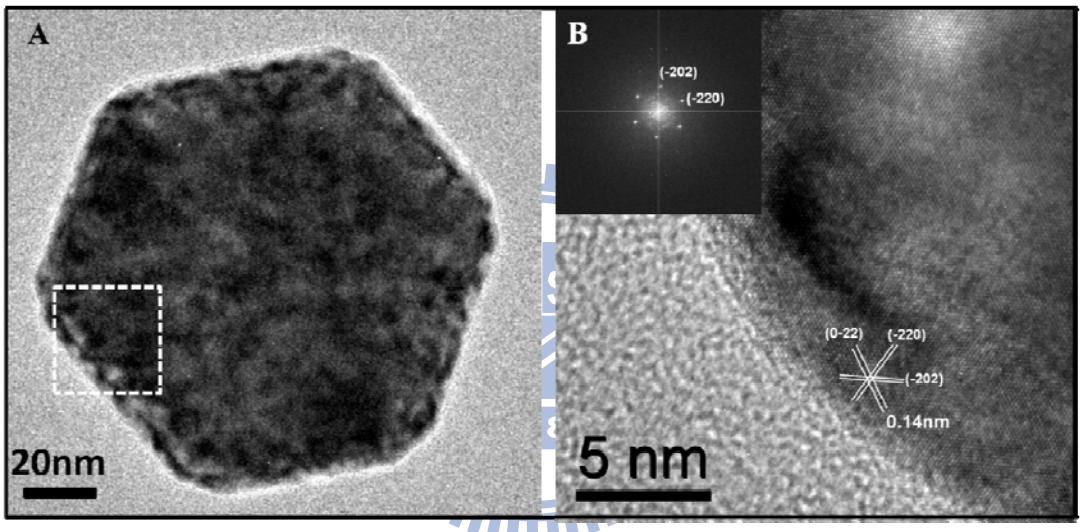

Figure 3.1.2. (A) TEM and (B) HRTEM images of a single Pd nanoplate obtained by using $PdCl_2$ of 0.3 mmol.

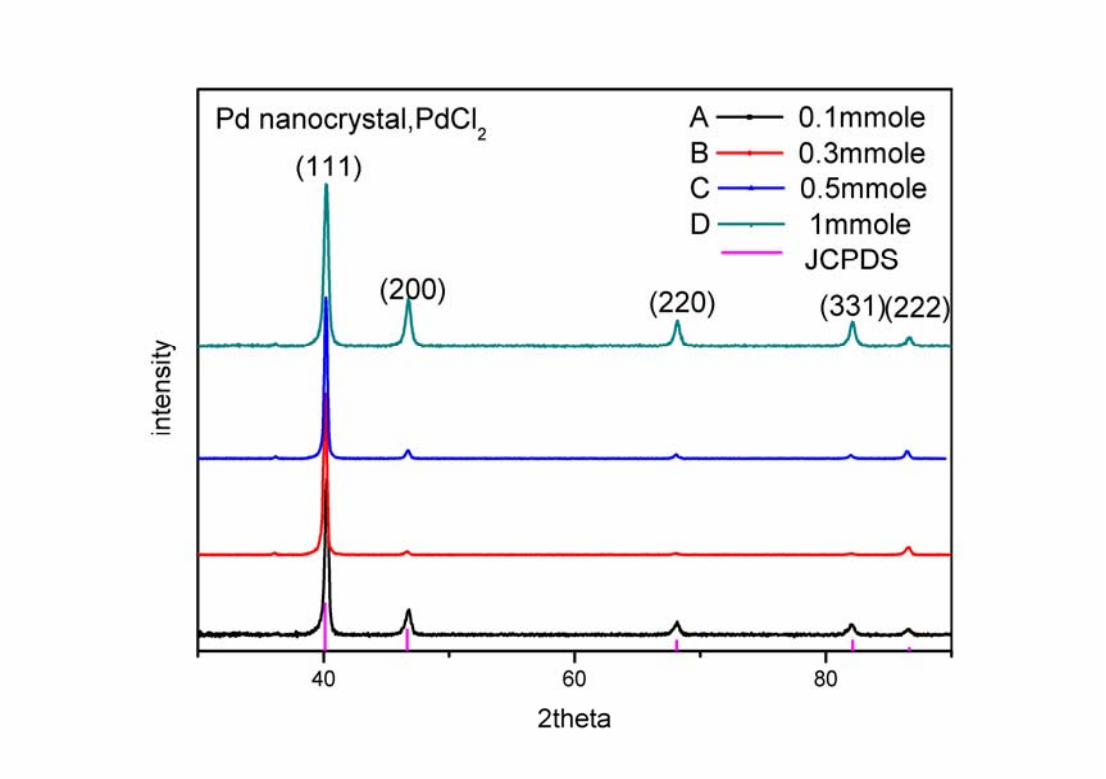

Figure 3.1.3. XRD patterns of Pd nanocrystals obtained by using $PdCl_2$ of various amounts.

Table 1. XRD intensity ratios of (111) to (200) peaks for Pd nanocrystals obtained by using $PdCl_2$ of various amounts.

$PdCl_2$ Amount (mmol)	**(111)**	**(200)**	**ratio**
(A) 0.1	**6200**	**995**	**6.23**
(B) 0.3	**35124**	**656**	**53.54**
(C) 0.5	**30090**	**1471**	**20.46**
(D) 1.0	**7054**	**2057**	**3.43**
Ref. Pd (from JCPDS)	**999**	**436**	**2.29**

These Pd nanocrystals were then analyzed in the electrochemical

system to test their electrocatalytic activity toward formic acid oxidation and hydrogen adsorption/desorption. For the direct formic acid fuel cell, potential (onset potential, forward peak potential) and current (peak current density, I_f/I_b) are the two important factors that can be used to evaluate the activity of the catalyst. For the formic acid oxidation, a more negative potential in the onset and forward peaks means that the reaction may be easily triggered and occur more readily, which can be attributed to the higher activity of the catalyst. On the other hand, a high current density in the forward peak is desirable for efficient catalyst since a high reaction rate is expected therein. The novel metal-catalyzed formic acid oxidation process mainly follows a dual-pathway mechanism.[25] The first reaction pathway is the direct oxidation (pathway 1) that occurs via a dehydrogenation reaction, without forming CO as a reaction intermediate. The second one (pathway 2) forms adsorbed CO as a reaction intermediate by dehydration. The two pathways can be described as follows:

Pathway1 : $HCOOH \rightarrow CO_2 + 2H^+ + 2e^-$

Pathway 2 : $HCOOH \rightarrow -CO_{ads} + H_2O \rightarrow CO_2 + 2H^+ + 2e^-$

In a typical CV plot for formic acid oxidation by using novel metal as

catalyst, the forward peak means the oxidation of formic acid. The backward peak however represents the adsorption of CO on catalyst surface, which causes an incomplete oxidation of formic acid to reduce the activity of catalyst. As a result, when the current of backward peak (I_b) in the CV plot is high, the issue of CO poisoning in catalyst gets serious. The ratio of currents of forward peak to backward peak (I_f/I_b) could thus be viewed as an index to evaluate the activity of catalyst toward formic acid oxidation. Figure 3.1.4 compares the CV results of the three Pd nanocrystals used for formic acid oxidation. The potential of the forward peak for the three samples was in the order of A (0.09V) > C (0.02V) > B (-0.05V). Samples of A and B had roughly the same forward peak current density, which is a little larger than C. We here concluded that sample B had the best electrocatalytic activity toward formic acid oxidation since it can catalyze the reaction at a low potential while a high reaction rate can still be maintained.

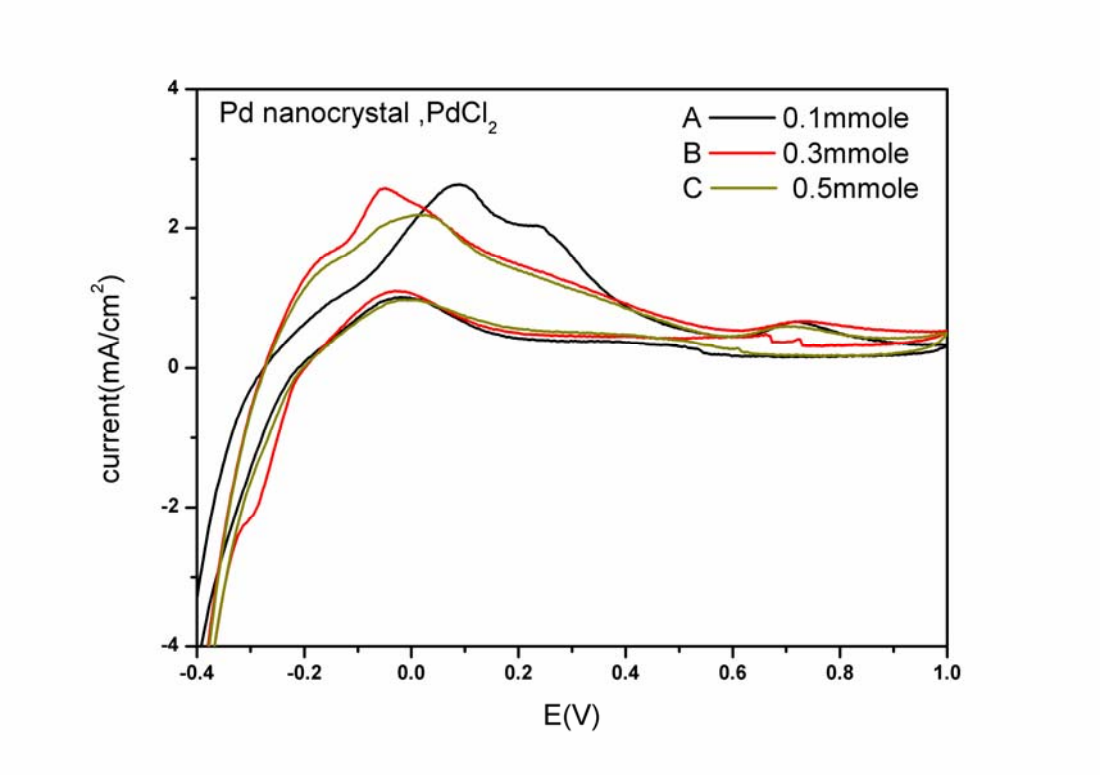

Figure 3.1.4. CV plots for Pd nanocrystals obtained by using $PdCl_2$ of (A) 0.1, (B) 0.3 (C) 0.5 mmol. The CVs were recorded in the solution of 2.0M HCOOH + 0.5M $HClO_4$ with a scan rate of 10mV/s.

To evaluate the electrocatalytic activity of Pd nanocrystals in a more general situation, we determined their electrochemically active surface areas (EASAs) through recording their CV plots in 0.1M H_2SO_4 electrolyte.[26] The value of EASA can be calculated from the CV data according to the following equation: $EASA = \frac{Q_H}{[Pd] \times C}$

, where Q_H is the Coulombic amount associated with the peak area, [Pd] is the mass of Pd loaded, and C is the quantity of electricity when hydrogen molecules are adsorbed on Pd with a homogeneous and single

layer. The CV results were shown in Figure 3.1.5 and the calculated EASAs for the three Pd nanocrystal samples were summarized in Table 2. It can be seen that samples of B and C have higher EASAs than sample A, which was attributed to the higher numbers of (111) planes at their faces that may show preference for hydrogen adsorption.

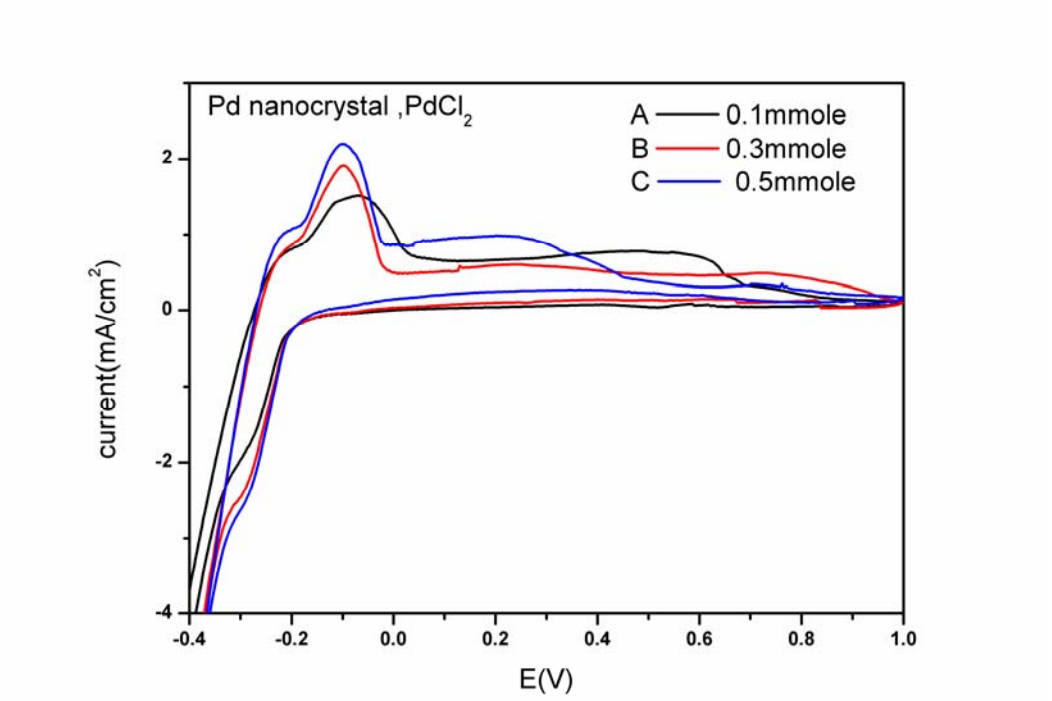

Figure 3.1.5. CV plots for Pd nanocrystals obtained by using $PdCl_2$ of (A) 0.1, (B) 0.3 (C) 0.5 mmol. The CVs were recorded in the solution of 0.5M H_2SO_4 with a scan rate of 10mV/s.

Table 2. Calculated EASAs for the three Pd nanocrystals.

Catalyst	Q_H(mC cm^{-2})	Q_H/[Pd](C g^{-1})	EASA(m^2g^{-1})
A	16.53	330.66	157.46
B	22.46	449.28	213.94
C	24.36	487.28	232.04

3.2 Effects of NaCl and NH_4OH Additions

Use of organic surfactants and polymers as additives in nanocrystal synthesis has been a popular method for achieving morphological control. Inorganic species would play an important role and work as effectively as organic surfactants.[27] For the polyol synthesis of nanocrystals, inorganic ions are expected to have a more significant influence on the growth of nanocrystals than organic polymer surfactants because of their relatively smaller sizes and the possible formation of complexes with the species in solution. The addition of inorganic ions may also induce the anisotropic growth of nanocrystals. Since $PdCl_2$ was not particularly soluble in water at room temperature, we added NaCl or NH_4OH along with $PdCl_2$ into water to increase the mobility of Pd^{2+} ions through the formation of complexes. The morphology of the resulting products was then investigated and compared.

3.2.1 Addition of NaCl with Various Amounts

When NaCl solution was added dropwise into $PdCl_2$ solution, the color of the solution changed from brown to brick red. This means that NaCl was reacted with $PdCl_2$ to form $PdCl_4^{2-}$ complexes.[28] Addition of NaCl at the reaction temperature of 100℃ produced Pd nanoplates with increasing percentage of triangular plates relative to the hexagonal plates. The role of NaCl in the growth of Pd at 100℃ was thus believed to increase the yield of triangular plates in the product. However, when the synthesis was performed at 75℃, the addition of NaCl resulted in the formation of Pd nanocrystals with polyhedral shapes. The morphology of the resulting nanocrystals was investigated with SEM and shown in Figure 3.2.1. Note that when adding NaCl of a small amount of 0.1 mL in the reaction at 75℃, an increase in the percentage of tiny triangular plates was again observed. Nevertheless, the morphology of Pd nanocrystals was turned into polyhedrons as the amount of NaCl was further increased to 0.5 and 1.0 mL. The corresponding TEM and HRTEM analyses in Figure 3.2.2 reveal the octahedral feature of these nanocrystals. Besides, the as-synthesized octahedrons of Pd were single-crystalline with a clear lattice fringe of (111) plane observed at their edge region.

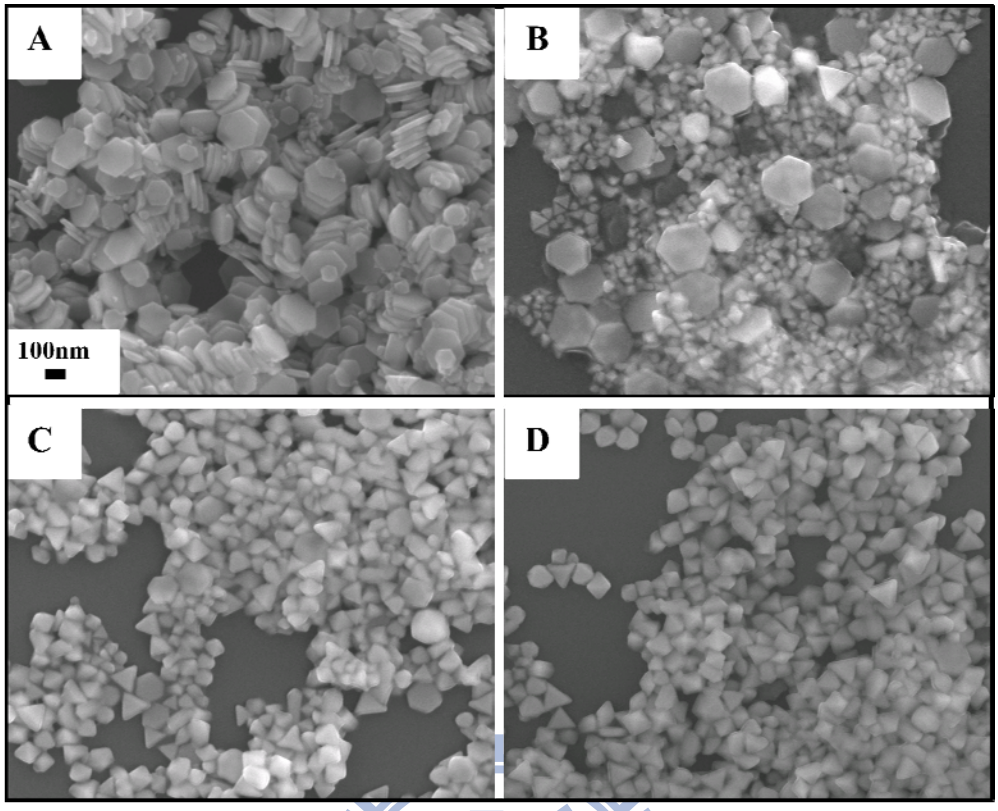

Figure 3.2.1. SEM images of Pd nanocrystals obtained with the addition of NaCl of various amounts. (A) 0, (B) 0.1, (C) 0.5, and (D) 1.0 mL.

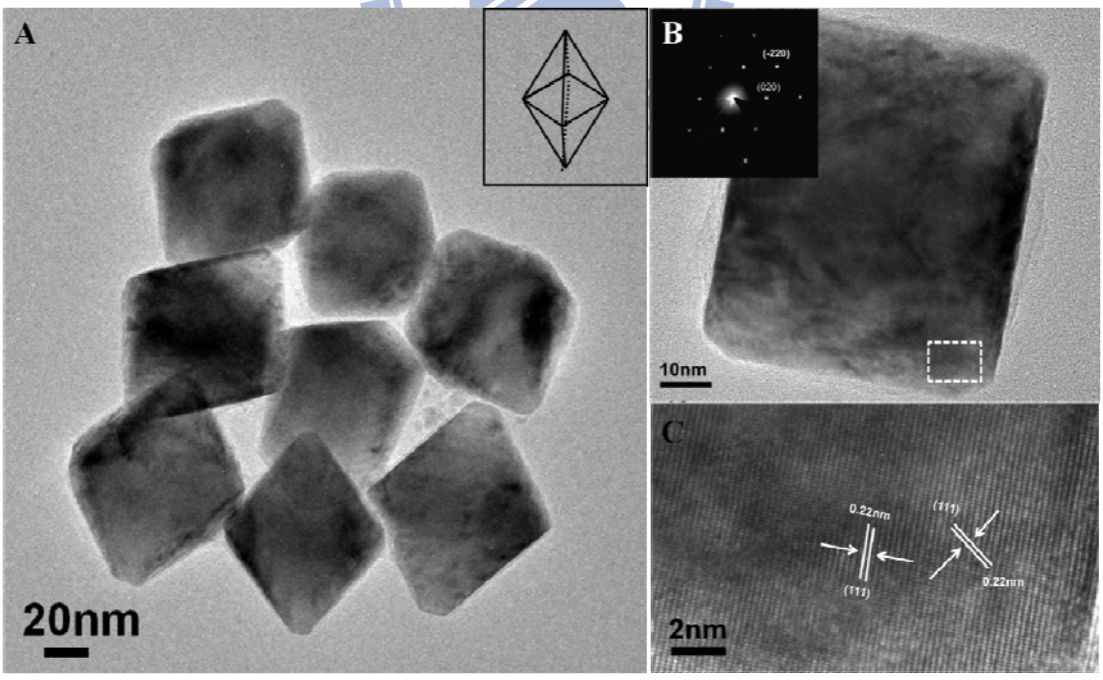

Figure 3.2.2. (A) TEM image, (B) SAED pattern and (C) HRTEM image of Pd octahedrons obtained with the addition of 1.0 mL NaCl. Inset of (A) illustrates the octahedron feature of nanocrystals.

XRD patterns of the three Pd nanocrystals obtained with the addition of NaCl were then taken and the results were shown in Figure 3.2.3. All of these samples could be indexed as the FCC crystal of Pd. Besides, an increase in the intensity ratio of (111) to (200) peaks was observed in the products when increasing the NaCl amounts. Together with the results of SEM and TEM investigations, we suggested that the octahedral structures of nanocrystals obtained with the addition of NaCl of 0.5 and 1.0 mL were enclosed by eight equivalent {111} faces.

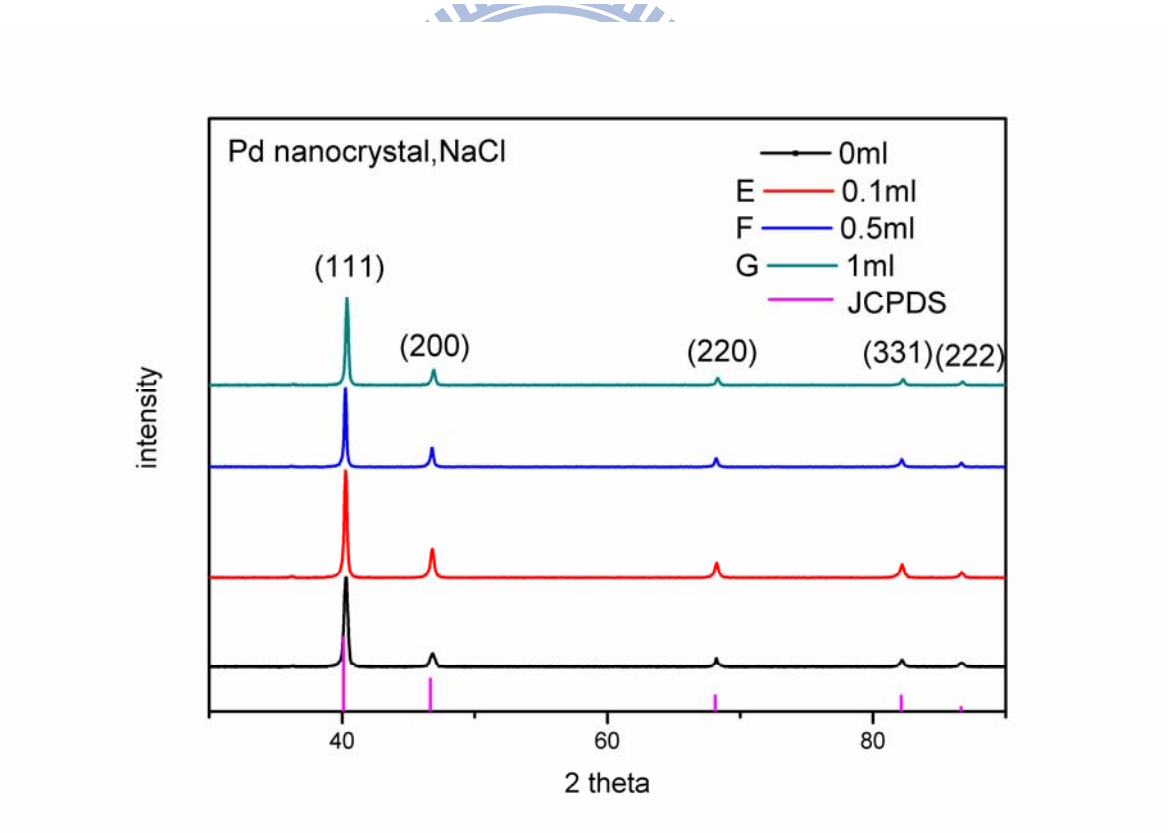

Figure 3.2.3. XRD patterns of Pd nanocrystals obtained with the addition of NaCl of various amounts.

Table 3. XRD intensity ratios of (111) to (200) peaks for Pd nanocrystals obtained with the addition of NaCl of various amounts.

NaCl Amount (ml)	(111)	(200)	ratio
(E) 0.1	17617	4818	3.66
(F) 0.5	14480	3911	3.70
(G) 1.0	11394	2019	5.64

Figure 3.2.4 displays the CV results of Pd nanocrystals obtained with the addition of NaCl for formic acid oxidation. Among the three samples, sample G was the best in catalyzing the formic acid oxidation since a lowest forward peak potential (0.15 V) with highest current density was attained. This outcome indicated that polyhedral shapes of Pd had good catalytic effects on the formic acid oxidation. The EASAs of the three samples were also calculated through recording their CV plots in 0.1M H_2SO_4 electrolyte. The resulting CV plots and the calculated EASA values were displayed in Figure 3.2.5 and Table 4, respectively. It can be seen that sample G had the highest EASA, which was again attributed to the {111} planes that enclosed its octahedral feature.

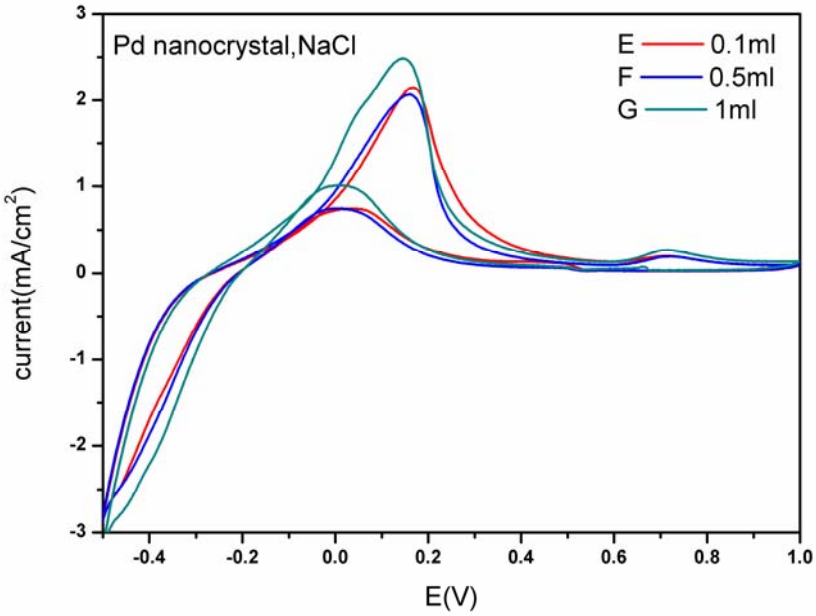

Figure 3.2.4. CV plots for Pd nanocrystals obtained with the addition of NaCl of (E) 0.1, (F) 0.5, (G) 1.0 mL. The CVs were recorded in the solution of 2.0M HCOOH + 0.5M $HClO_4$ with a scan rate of 10mV/s.

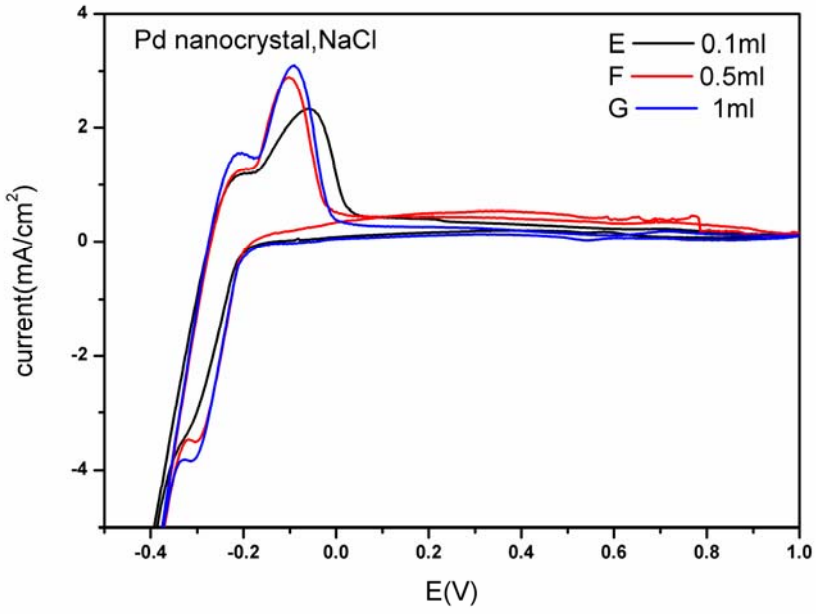

Figure 3.2.5. CV plots for Pd nanocrystals obtained with the addition of NaCl of (E) 0.1, (F) 0.5, (G) 1.0 mL. The CVs were recorded in the solution of 0.5M H_2SO_4 with a scan rate of 10mV/s.

Table 4. Calculated EASAs for the three Pd nanocrystals.

catalyst	Q_H(mC cm-^{2})	Q_H/[Pd](C g^{-1})	EASA (m^2 g^{-1})
E	29.56	591.26	281.55
F	31.67	633.34	301.59
G	40.68	813.68	387.47

3.2.2 Addition of NH_4OH with Various Amounts

In addition to NaCl, NH_4OH may also help to dissolve $PdCl_2$ by forming the complexes through the binding of Pd^{2+} to NH_3. Figure 3.2.6 shows the TEM images of Pd nanocrystals obtained with the addition of NH_4OH of various amounts. Note that the synthesis was performed at 85℃ here. The TEM images clearly reveal a change in morphology of Pd as the amount of NH_4OH was gradually increased. The results were completely different from the case of NaCl addition, which was believed to be due to the distinct complexes of Pd^{2+} formed. We observed that $Pd(NH_3)_4^{2+}$ complexes in the NH_4OH case exhibits a much slower reaction rate than $PdCl_4^{2-}$ complexes in the NaCl case. The reaction kinetics can then be slowed down by the addition of NH_4OH, thereby altering the growth of Pd to form nanocrystals with different shapes. This effect was pronounced when NH_4OH of 0.3 mL was added, resulting in

the formation of tiny polyhedrons. As the amount of NH_4OH was further increased to 1.0 mL, porous nanocrystals with a lot of tiny cavities were obtained. XRD patterns of these Pd nanocrystals were also taken and the results were shown in Figure 3.2.7. All of these samples could also be indexed as the FCC crystal of Pd.

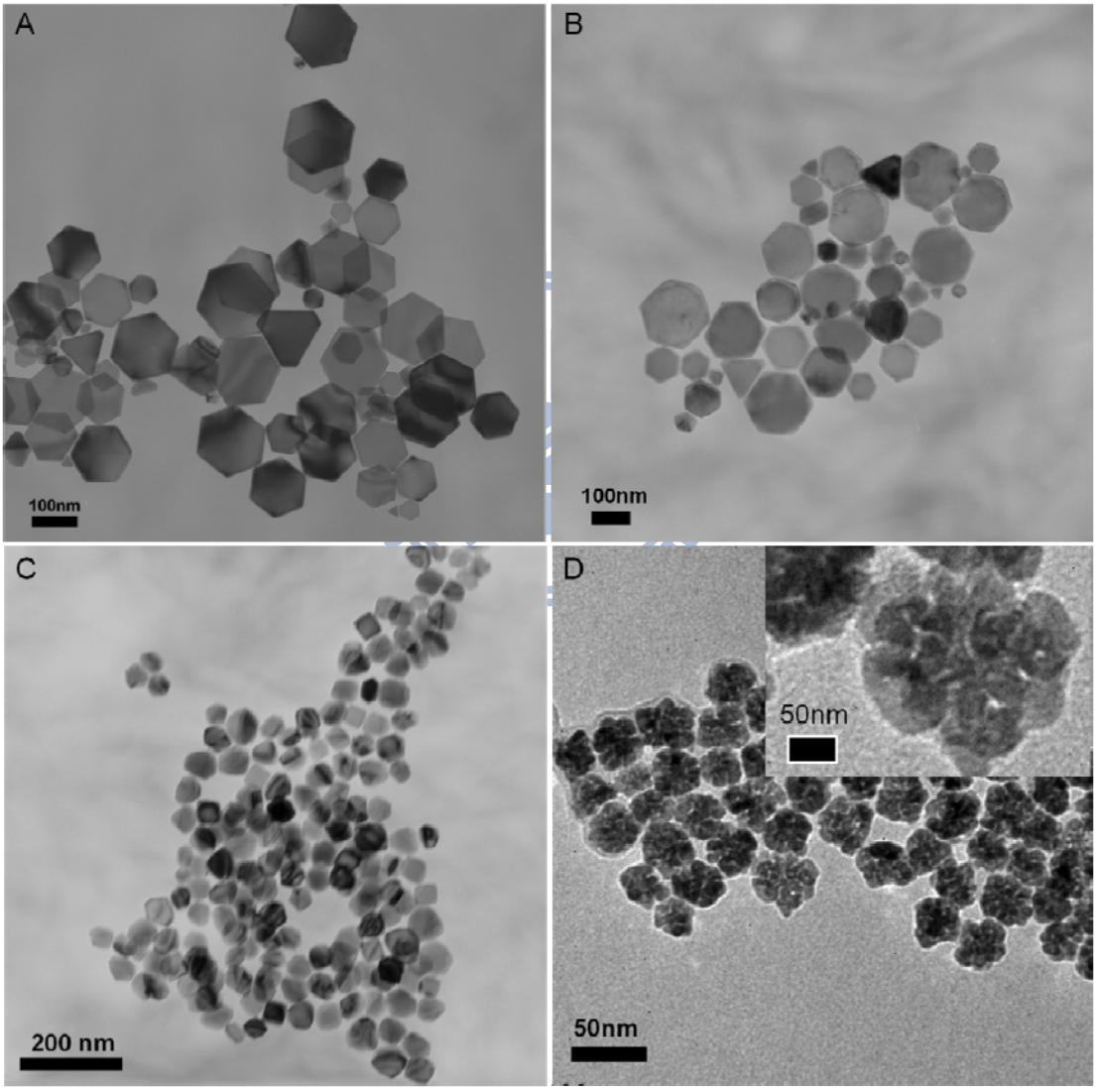

Figure 3.2.6. TEM images of Pd nanocrystals obtained at 85℃ with the addition of NH_4OH of (A) 0, (B) 0.1, (C) 0.3, and (D) 1.0 mL.

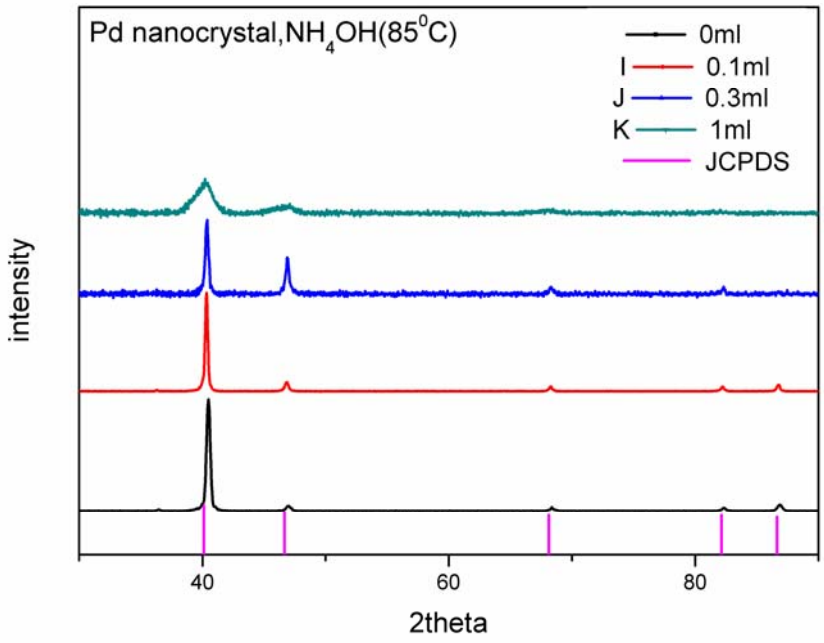

Figure 3.2.7. XRD patterns of Pd nanocrystals obtained at 85℃ with the addition of NH_4OH of various amounts.

The morphology of the resulting Pd nanocrystals obtained with the addition of NH_4OH can be further tailored if the synthesis was performed at 100℃. As displayed in Figure 3.2.8, hollow-like structures of Pd can be fabricated at 100℃ with the addition of 1.0 mL NH_4OH. The corresponding XRD patterns shown in Figure 3.1.9 also reveal the FCC crystal structure of Pd for the four samples.

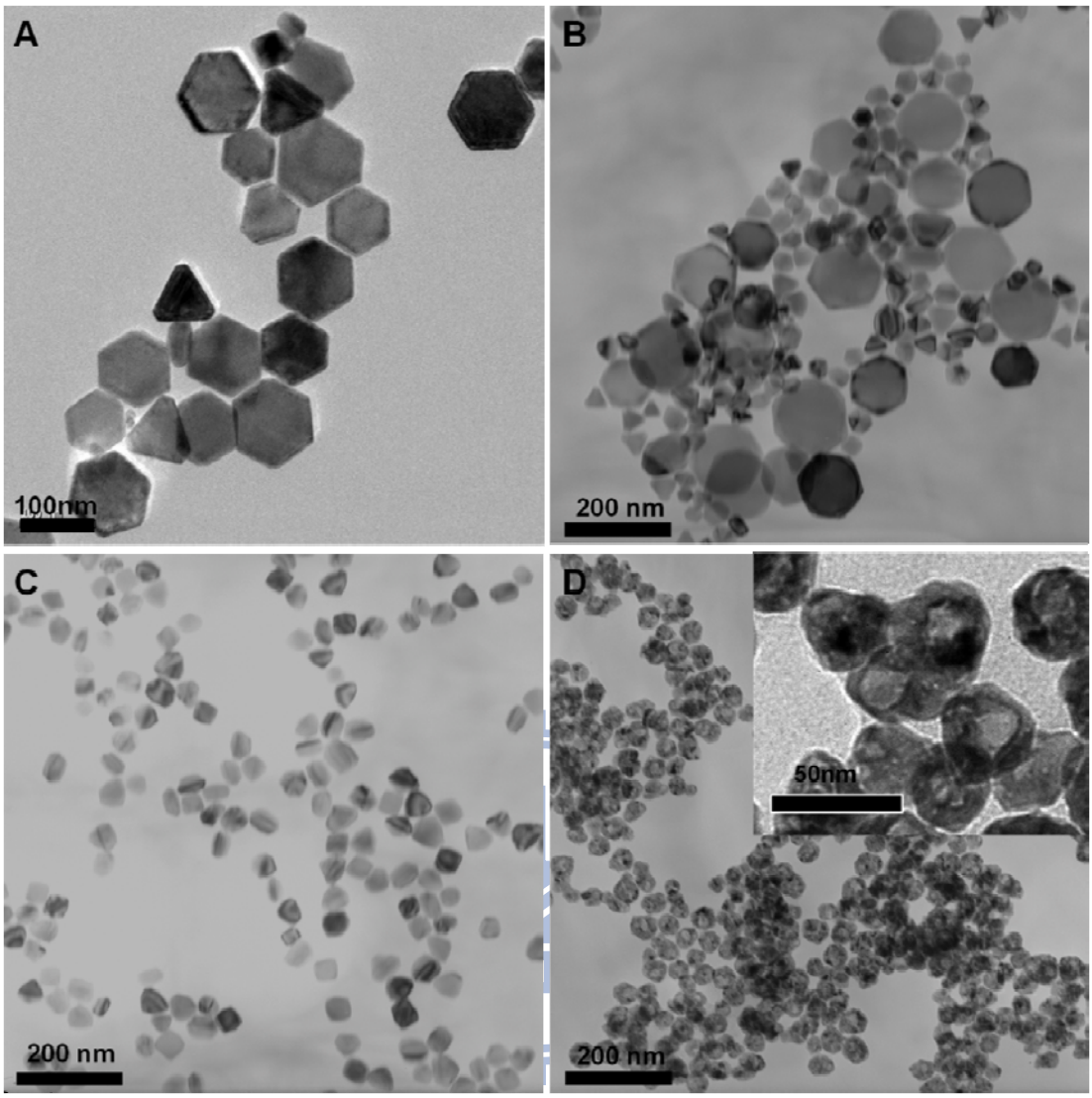

Figure 3.2.8. TEM images of Pd nanocrystals obtained at 100℃ with the addition of NH_4OH of (A) 0, (B) 0.1, (C) 0.3, and (D) 1.0 mL.

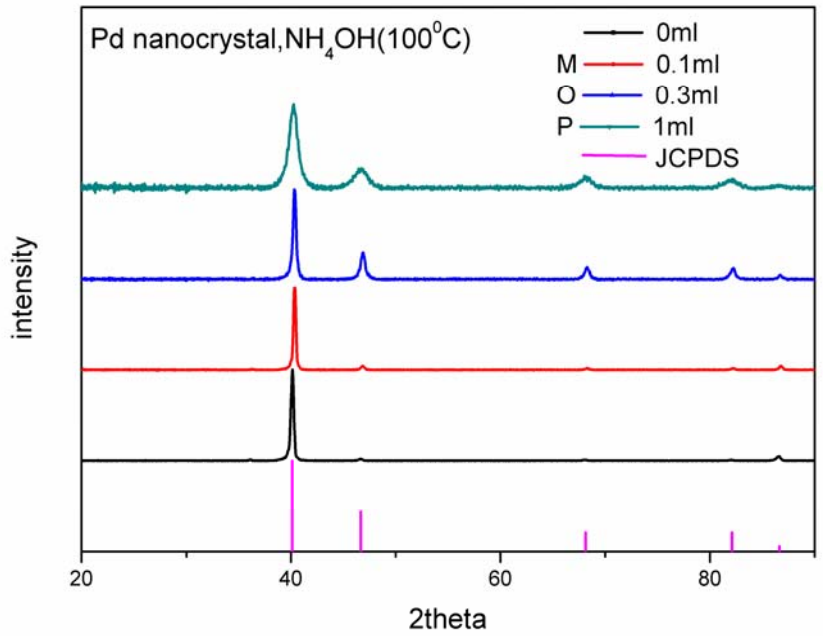

Figure 3.2.9. XRD patterns of Pd nanocrystals obtained at 100℃ with the addition of NH_4OH of various amounts.

3.2.3 Comparison of Electrocatalytic Activity

The various nanocrystals of Pd we collected in this work were then compared in the formic acid oxidation and hydrogen adsorption/desorption. The samples included nanoplates (B), octahedrons (G), porous nanocrystals (K), hollow nanocrystals (P), and commercial Pd particles. Figure 3.2.10 shows the typical CV plots for these samples used for formic acid oxidation. The information about the forward peak potentials, the I_f/I_b ratios, and the EASA values for these samples was

summarized in Tables 5 and 6. Among all the samples tested, hollow nanocrystals possess the highest current density of formic acid oxidation and the largest I_f/I_b ratio, demonstrating that they could be promisingly used as highly-efficient CO-resistant electrocatalyst in the direct formic acid fuel cell. Furthermore, as compared to the commercial Pd particles, the four types of Pd nanocrystals all exhibited superior activities toward hydrogen adsorption/desorption, revealing their catalytic potential in relevant electrochemcial reactions.

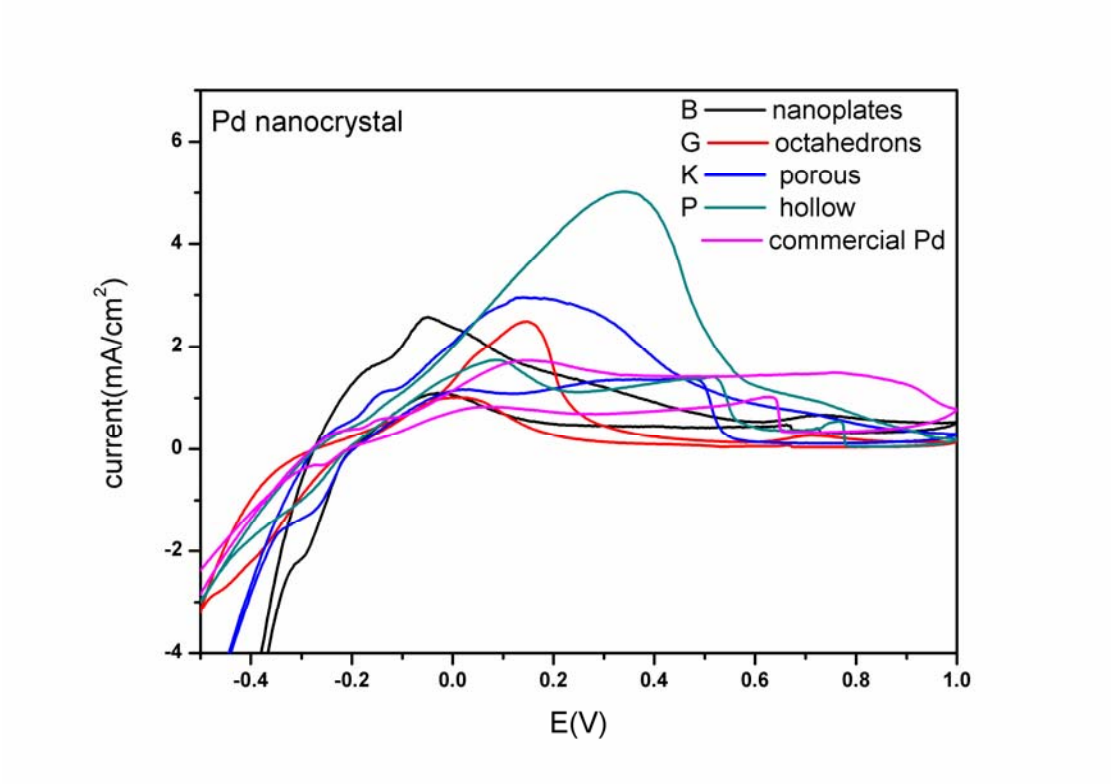

Figure 3.2.10. CV plots for various Pd nanocrystals: (B) nanoplates, (G) octahedrons, (K) porous nanocrystals, (P) hollow nanocrystals. The CVs were recorded in the solution of 2.0M HCOOH + 0.5M $HClO_4$ with a scan rate of 10mV/s.

Table 5. Electrocatalytic activities of various Pd nanocrystals for formic acid oxidation.

catalyst	Onset potential (V)	Forward peak potential (V)	I_f/I_b
B, nanoplates	**-0.11**	**-0.05**	**2.35**
G, octahedrons	**-0.04**	**0.15**	**2.48**
K, porous nanocrystals	**-0.10**	**0.15**	**2.13**
P, hollow nanocrystals	**-0.15**	**0.34**	**3.57**
commercial Pd	**-0.10**	**0.15**	**1.70**

Table 6. Calculated EASAs for various Pd nanocrystals: : (B) nanoplates, (G) octahedrons, (K) porous nanocrystals, (P) hollow nanocrystals.

catalyst	Q_H(mC cm-^{2})	Q_H/[Pd](C g^{-1})	EASA (m^2 g^{-1})
B	22.46	449.28	213.94
G	40.68	813.68	387.47
K	17.65	352.92	168.06
P	22.87	457.36	217.79
comercial Pd	5.07	101.32	48.25

3.3 SERS Properties of Pd Nanocrystals

Since Pd nanoplates and octahedrons obtained in this work were anisotropically shaped, their specific facets may focalize the electromagnetic field, making them an ideal platform for SERS ultradetection of analytes. Figure 3.3.1 shows the SERS spectra of MB adsorbed on the substrates containing various Pd nanocrystals acquired under the excitation of 632.8 nm laser. Notably, the SERS signals could only be registered when MB was adsorbed on the substrates containing nanoplates and octahedrons. No signals were acquired from the equivalent configuration with substrate containing porous nanocrystals. This demonstration reveals that the present Pd nanoplates and octahedrons can serve efficient SERS enhancers toward relevant Raman-sensitive analytes.

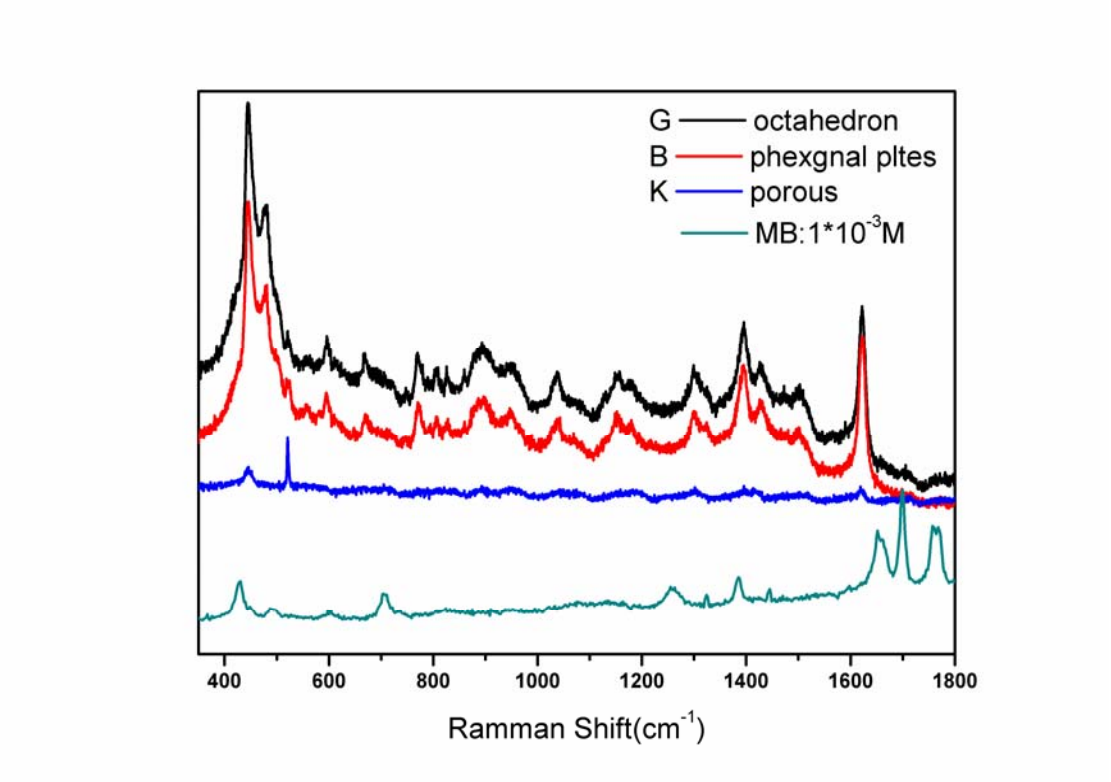

Figure 3.3.1 SERS spectra of MB adsorbed on substrates containing various Pd nanocrystals.

Chapter 4. Conclusions

We have successfully synthesized various Pd nanocrystals including nanoplates, octahedrons, porous nanocrystals, and hollow nanocrystals in the PVP-assisted chemical reduction process. The synthesis involved only the use of $PdCl_2$ as the precursor, PVP as the reducing and stabilizing agents, and a specific salt like NaCl or NH_4OH as the additive. By modulating the relevant reaction conditions such as the amount of $PdCl_2$, the amount of additive, and the reaction temperature, we were able to obtain Pd nanocrystals with controlled morphologies. Pd hollow nanocrystals could be promisingly used as the highly-efficient CO-resistant electrocatalyst in the direct formic acid fuel cell. Furthermore, as compared to the commercial Pd particles, the four types of Pd nanocrystals all exhibited superior electrocatalytic activities toward hydrogen adsorption/desorption, revealing their catalytic potential in relevant electrochemical reactions. The results of SERS analyses demonstrate the potential of the anisotropically-shaped Pd of nanoplates and octahedrons as an active platform for Raman-sensitive analyte molecules.

References

1. Hatakeyama, Y.; Umetsu, M.; Ohara, S.; Kawadai, F.; Takami, S.; Naka, T.; Adschiri, T. *Adv. Mater.* **2008**, *20*, 1122.
2. Tanaka, H.; Uenishi, M.; Taniguchi, M.; Tan, I.; Narita, K.; Kimura, M.; Kaneko, K.; Nishihata, Y.; Mizuki, J. *Catal. Today*, **2006**, *117*, 321.
3. Xiao, C.; Ding, H.; Shen, C.; Yang, T.; Hui, C.; Gao, H.-J. *J. Phys. Chem. C.* **2009,** *113*, 13466.
4. McLellan, J. M.; Xiong, Y.; Hu, M.; Xia,Y. *Chem. Phys. Lett.* **2006,** *417*, 230.
5. Liu, H. P.; Ye, J. Q.; Xu, C. W.; Jiang, S. P.; Tong, Y. X. *J. Power Sources.* **2008**, *177*, 67.
6. Larsen, R.; Ha, S.; Zakzeski, J.; Masel, R. I. *J. Power Sources.* **2006**, *157*, 78.
7. Xiong, Y.;, Cai, H.; Wiley, B. J.; Wang, J.; Kim, M. J.; Xia, Y. *J. Am. Chem. Soc.* **2007**, *129*, 3665.
8. Huang, X.; Zhang H.; Guo C.; Zhou, Z.; Zheng, N. Angew. *Chem. Int. Ed*. **2009**, *48*, 1.
9. Xiong, Y.; McLellan, J. M.; Chen, J.; Yin, Y.; Li, Z.-Y.; Xia, Y. *J. Am. Chem. Soc***. 2005**, *127*, 17118.
10. Niu, W.; Zhang, L.; Xu, G. *Nano Lett.* **2010**, *4*, 1987.
11. Watt, J.; Cheong S,; Toney M. F.; Ingham B.; Cookson J.; Bishop P.T.; Tilley R. D. *Nano Lett*. **2010** , *4* , 396.
12. Adams, B. D.; Wu, G.; Nigro, S.; Chen, A. *J. Am. Chem. Soc.* **2009**, *131*, 6930.
13. Narayanan, R.; El-Sayed, M.A. *J. Am. Chem. Soc*. **2003**, *125*, 8340

14. Calvo, F.; Carre , A. *Nanotechnology.* **2006**, *17*, 1292

15. Adzic, R.R.; Tripkovic, A.V.; O'Grady, W. *Nature*. **1982**, *296* ,137

16. Sun, S.; Yang, Y. *J. Electroanal. Chem.* **1999**, *467* , 121

17. Ha, S.Y.; Larsen, R. ; Masel, R.I. *J. Power Sources.* **2005** , *144* ,28.

18. Zhang, L.; Lu, T.; Bao, J.; Tang, Y.; Li, C. *Electrochem. Commun*. **2007**, *8*, 1625.

19. Solla-Gullon, J.; Vidal-Iglesias ,F.J.; Lopez-Cudero, A.; Garnier, E.; Feliu, J.M.; Aldaz, A. *Phys. Chem. Chem. Phys*. **2008,** *10*, 3689.

20. Wang, R.; Liao, S.; Ji. S. *Electrochem. Commun.* **2010**, *12*, 219.

21. Hoshi, N.; Kida, K.; Nakamura, M.; Nakada, M.; Osada, K. *J. Phys. Chem. B* .**2006,** *110*, 12480.

22. Manzanares, M. I.; Pavese, A. G.; Solis, V. M. *J. Electroanal.Chem.* **1991**, *310*, 159.

23. McLellan, J. M.; Xiong,Y.; Hu, M.; Xia,Y. *Chem. Phy. Lett*. **2006**, *417* , 230.

24. Xiong, Y.; Washio, I.; Chen, Ji.; Cai, H,; Li, Z.-Y.; Xia,Y. *Langmuir,* **2006,** *22*, 8563.

25. Feliu, J.M.; Herrero, E.; Vielstich, in:W.; Gasteiger, H.A.; Lamm, A. *Handbook of Fuel Cells*, **2003**, *2*, 679.

26. Mazumder, V.; Sun, S. *J. Am. Chem. Soc.* **2009,** *131*, 4588.

27. Herricks, T.; Chen, J.; Xia, Y. *Nano Lett*. **2004** , *4*, 12.

28. Li, C.; Sato, R.; Kanehara, M.; Zeng, H.; Bando, Y.; Teranishi T. *Angew. Chem. Int. Ed*. **2009**, *48*, 6883.